scientific reports

Check for updates

OPEN

Experimental evolution of active Brownian grains driven by quantum effects in superfluid helium

Oleg F. Petrov✉, Roman E. Boltnev & Mikhail M. Vasiliev

Complex structures, consisting of a large number of interacting subsystems, have the ability to self-organize and evolve, when the scattering of energy coming from the outside ensures the maintenance of stationary ordered structures with an entropy less than the equilibrium entropy. One of the fundamental problems here is the role of quantum phenomena in the evolution of macroscopic objects. We provide experimental evidence for the active Brownian motion and evolution of structures driven by quantum effects for micron-sized grains levitating in superfluid helium. The active Brownian motion of grains was induced by quantum turbulence during the absorption of laser irradiation by grains. The intensity of Brownian motion associated with quantum vortices increased by 6–7 orders of magnitude compared to the values from the Einstein formula. We observed the grain structures in a state far from thermodynamic equilibrium and their evolution to more complex organized structures with lower entropy due to the quantum mechanism of exceedingly high entropy loss in superfluid helium.

The observation of processes in nature and social phenomena shows that many complex structures, consisting of a large number of interacting subsystems, under certain conditions have the ability to self-organize and evolve. The structures are called dissipative, provided that the scattering of energy coming from outside provides a stationary ordered structure with an entropy less than the equilibrium one. The dissipative structures are capable of self-organization and evolution while increasing the flow of entropy into the environment[1–4].

Self-organization is considered as an elementary process of evolution consisting of an unlimited sequence of self-organization processes and leading to the formation of more complex structures of the entire system. Along with dissipative self-organization, there are other types, such as conservative self-organization (formation of crystal structures, biopolymers, etc.) and dispersive self-organization (formation of soliton structures)[1,2]. Note that living systems are distinguished among dissipative structures[1–4]. The basic feature of such systems is spontaneous evolution, which is the development of more complex forms due to a sequence of self-organization processes[1,2,4,5]. The fundamental problem here is the thermodynamics of prebiological evolution, when a prebiological system can evolve through a whole sequence of transitions leading to a hierarchy of increasingly complex and organized states. These transitions can occur only in nonlinear systems far from thermodynamic equilibrium[4,6].

Here, entropy is a key physical quantity when describing self-organization; it serves as a measure of disorder so that a decrease in entropy in the system leads to self-organization. The entropy of the system can decrease if the system exports entropy so that the export per unit of time exceeds the corresponding production of entropy in the system. This process requires an entropy pump. To drive the pump, as for driving any machine, a consumable free energy or free enthalpy is required, which the pump can take from external or internal sources[1,2].

In recent years, active Brownian motion has attracted great interest in biology, physics, sociology, material science, and epidemiology. While passive Brownian grains are in thermal equilibrium with their environment, active Brownian grains are able to absorb energy from their environment and turn it into their kinetic energy that displaces them from thermodynamic equilibrium[7]. Thus, the systems of active Brownian grains can be considered as open systems, and the structures of grains themselves are systems far from thermodynamic equilibrium.

Active Brownian grains can be charged grains, suspended in plasma or levitated in a cryogenic liquid (cryogenic colloid), the kinetic motion of which is induced by laser radiation[8,9]. In this case, the state of grains is maintained by the free energy of radiation.

One of the fundamental problems in modern physics is the role of quantum effects at the macroscopic scale (in the macroscopic world)[10] and, in particular, in the evolution of macroscopic structures of matter. Thus, a necessary condition for the evolution of dissipative structures is the outflow (export) of entropy into the environment.

Joint Institute for High Temperatures, Russian Academy of Sciences, Moscow 125412, Russia. ✉email: ofpetrov@ihed.ras.ru

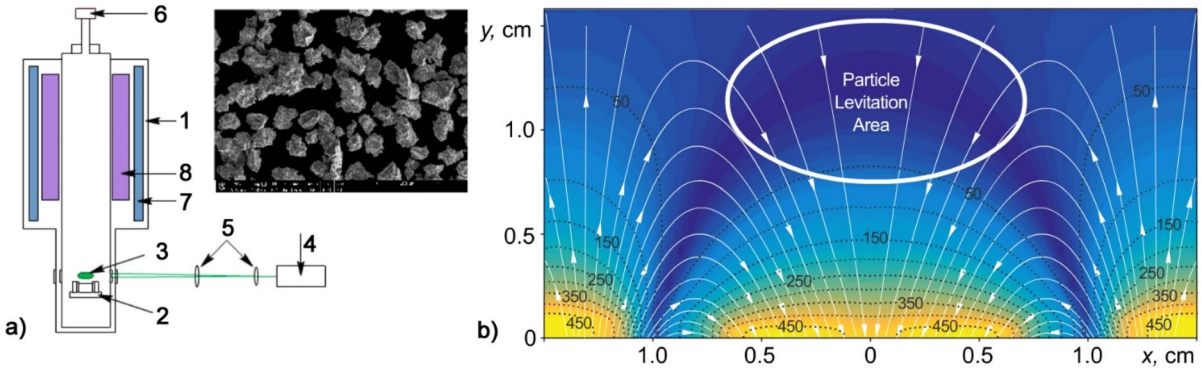

Figure 1. Experimental setup and magnetic trap: (**a**) Scheme of the experimental setup: 1—optical cryostat; 2—platform for the magnetic trap; 3—captured grains in the trap; 4—laser for illumination of $YBa_2Cu_3O_7$ grains in a trap; 5—lenses; 6—vacuum gauge; 7—bath with liquid nitrogen; 8—bath with liquid helium; (**b**) The distribution of the magnetic field (mT) in the trap for confining $YBa_2Cu_3O_7$ grains: the thin white lines correspond to the lines of force, and the black dashed lines correspond to the equipotential surfaces of the magnetic field with the denoted values (mT). Inset: Electron microscope image of $YBa_2Cu_3O_7$ grains.

Such export can be created, for example, by heat transfer due to radiation or by the mechanism of heat transfer in the environment. During heat transfer in condensed matter, an exceedingly high rate of heat (and entropy) loss is achieved in a quantum liquid (superfluid helium). Therefore, macroscopic phenomenon such as the evolution of colloidal systems in superfluid helium can be associated with quantum effects[11]. The mechanism of activity of Brownian grains in superfluid helium, when they absorb radiation energy and can be heated, can also have a quantum nature associated with the formation of quantum turbulence near the heated grain surface[12,13].

In this paper, we present the results of the experimental evidence of the evolution of the spatial structures of highly charged (up to 10^5 e) micron-sized grains levitating in a static magnetic trap[8,14–19] in superfluid helium ^{4}He at temperatures T_{He} = 1.7–2.18 K. The levitation of the grains made with high-temperature superconducting ceramics[20] is based on the well-known Meissner effect of expulsion of the magnetic field from the volume of the superconducting phase[21,22]. Such systems can be considered colloidal structures in a cryogenic liquid (cryogenic colloid)[8].

We observed the formation and evolution of a complex structure maintained far from equilibrium by the energy of laser radiation. The structure consisted of a cloud of single grains and spatially oriented chains with strong Coulomb and magnetic intergrain interactions. The absorption of light and heat release on the surface of grains at a certain laser power can initiate the appearance of quantum vortices in superfluid helium and the generation of quantum turbulence[12,13]. It is revealed that an increase in the power density of laser radiation increases the kinetic energy of the motion of grains and their diffusion coefficient by many orders of magnitude in comparison with the equilibrium values at the temperature of superfluid helium.

The study of the spatial structures of grains under the action of laser radiation has also been carried out in low-pressure gas discharges, both at room temperature and at temperatures of superfluid helium[23,24].

Surprisingly, another observed effect is the increase in the number and length of grain chains with the increase in the power density of laser radiation. It should be noted that an increase in the kinetic energy of grains in the chain structures in the low-pressure gas discharges leads to the destruction of chain structures and the transition of the system to a less ordered state[24,25].

Experiments

To study experimentally the strongly interacting Coulomb structures, a levitation of grains confined in an inhomogeneous stationary magnetic field is commonly employed[14,15]. Graphite, as a material with a great value of specific magnetic susceptibility, is of frequent use in experiments on grain confinement in nonuniform magnetic fields[16,17]. Under the conditions of laboratory experiments, at magnetic fields of ~ 2 T/mm, the authors obtained a cluster consisting of only a few graphite grains with sizes of several hundred microns. In experiments on board the International Space Station under microgravity conditions, the formation of an extended cluster of several thousand charged diamagnetic grains, tens and hundreds of microns in size, was observed[18]. The method of magnetic self-assembly of diamagnetic spheroids was also used by the authors to print living tissues[19].

We used a levitation of micron-sized grains confined in an inhomogeneous stationary magnetic field with induction B_m. Stable levitation of diamagnetic bodies occurs in the region of a local minimum of the magnetic field; however, under conditions of gravity, magnetic fields can be used without a local minimum (see Fig. 1). In this case, the force $F_d = (\chi_p V_p/\mu_o)\nabla(B_m^2)$ is balanced by gravity (here, μ_o vacuum permeability, χ_p magnetic susceptibility of grain material, and V_p grain volume[8,16–18]).

Experimental design. The main part of the experimental setup is a Janis SVT-200 optical helium cryostat with an operating temperature range of 1.5–273 K (see Fig. 1a). A special insert is placed in the central vertical channel of the cryostat, which is 62 mm in diameter. At the lower part of the insert, there is a platform for

installing magnets that form a magnetic trap. The platform is fixed at the level of the cryostat optical windows. A semiconductor thermometer TPK-1.5/60–22 is attached to the platform. The thermometer is operated with a temperature controller (Lake Shore 335).

In our work, an assembly of a pair of permanent axial magnets made of NdFeB was used as a magnetic trap. The outer ring, in the form of a ring with outer and inner diameters of 35 and 20 mm, respectively, had a height of 8 mm and a residual magnetic induction of 1.43 T. The inner cylinder, in the form of a cylinder with a diameter of 15 mm and a height of 5 mm, had a residual magnetic induction of 1.46 T. The induction vectors of the magnets in the assembly were directed in opposite directions. To maintain the mutual orientation of the magnets, an insert in the form of a ring made of a nonmagnetic material, stainless steel, was installed in the gap between them. The configuration accuracy of the magnets was ± 0.1 mm. Grains made of the high-temperature superconductor $YBa_2Cu_3O_7$ with a critical temperature of 93 K were injected into a trap, and the grain sizes ranged from 30 to 60 μm (see subplot in Fig. 1a). An injector was located 6 cm above the magnets. The injector holder, injector body and platform for magnets are made of a diamagnetic material—polyamide-6. When injected at temperatures higher than the critical temperature, grains fell onto magnets and were charged up to potential φ applied to magnets. The transition of $YBa_2Cu_3O_7$ grains to the superconducting state upon cooling led to the formation of a cloud captured in a magnetic trap (see in Fig. 1b the magnetic field distribution of the trap was measured with a digital magnetometer Aktakom ATE-8702) and to the appearance of spatial structures of grains in it.

The main elements of the diagnostic complex of the experimental setup were a high-speed digital video camera IDT X-Stream, a solid-state laser with a wavelength of $\lambda = 532$ nm with an output power up to 1.0 W and a personal computer with a package of specialized programs for grain detection, video recording, and video data processing. Visualization of grains levitating in a magnetic trap was carried out by illuminating them with an expanded laser beam, passing through the optical window of the cryostat. The grains illuminated by laser radiation were recorded using the video camera through the optical window of the cryostat located at an angle of 90° to the illuminating laser beam. The resulting video images were processed by specially developed computer programs, as a result of which we obtained the coordinates of the grains, as well as their trajectories $r_p(t)$, their velocity v_p, acceleration a_p and mean-square displacements $< \Delta r^2(t) >$.

Data analysis. For visualization, the laser radiation scattered by the grains is recorded by a video camera. The resulting video recording of grains in the structure is processed by the following software algorithm. First, static noise in the video image is detected and removed, and low- and high-frequency spatial noise is filtered. Next, the search for local maxima in the filtered image is performed. For each maximum, the weighted average coordinate and the integrated brightness of circles considered grains are determined, and then images with brightness values that are too low are deleted. Next, the search for grains on all frames of the video (to restore their trajectory) is carried out using the maximum likelihood method. Likelihood is calculated from the relative displacements of a grain from frame to frame and its brightness, taking into account the behavior of neighboring grains. Finally, the heuristic algorithm processes special cases (intersections and discontinuities of trajectories) and determines the final set of grain trajectories.

The analysis of the obtained video data makes it possible to determine the coordinates of single grains at each moment of time, while the analysis of the displacements of grains for the interframe interval gives the speed v_p of their motion. Based on the data about the velocities of all grains of a dusty system at each moment of time, it is possible to obtain the velocity distribution of grains and their average kinetic energy of grain motion $E_k = m_p v_p^2/2$.

Results and discussions

Grain levitation in the magnetic trap. In our experiments, the magnitude of the electric potential φ_p applied to the magnets was on the order of 20 V. As a result of the contact of the superconducting ceramic grains with the magnets, grains gained a charge Z_p, the value of which can be estimated as $Z_p = 4\pi\varepsilon_o\varphi_p(d_p/2)$, where $\varepsilon_o = 8.85 \cdot 10^{-12}$ F/m is the dielectric constant. For grains with an average diameter of $d_p \approx 40$ μm, the value of the charge Z_p does not exceed ($Z_p \lesssim 2.7 \cdot 10^5\, e$), where e is the electron charge. As a result, the formation of a complex spatial colloidal structure by grains confined in a magnetic trap in the form of a "jelly fish" was observed, the "core" of which was rather loose, and the upper part ("umbrella") consisted of a cloud of space-oriented chains and single grains, illuminated by laser radiation of various powers $I_L = 0.1$–1.0 W (see Fig. 2 and Supplementary InformationVideo file “V1.avi”). The characteristic vertical and transverse dimensions of the colloidal structure were approximately 8 and 20 mm, respectively (the cross-sectional area S_{str} of the structure was approximately 1.6 cm^2). Such a system of oriented chains is typical for nematic liquid crystals[26]. The number of grains in the chains varied from 5–7 to 15–20, and the average distance between grains in the chains was in the range of 40–70 microns.

The power density of laser radiation $\dot{Q}_L = I_L/S_L$ (where S_L is the cross-sectional area of the laser beam) on the grain surface varied within $\dot{Q}_L \approx 0.37$–2.7 W/cm^2. The power of heat released on one grain could be on the order of $I_L((\pi d_p^2/4)/S_L) \approx 3$ - 24 μW for grains with an average diameter of $d_p \approx 40$ μm, provided that the absorption coefficient of radiation of the grain material in the visible spectrum is 0.7. In this case, the power density of heat release $\dot{Q}_p$ on the surface of the grains is in the range 0.26–1.9 W/cm^2. The power of local heat release depends on the size of the grain and is proportional to its area; therefore, in experiments[27–29], it was 3–4 orders of magnitude lower.

The formation of chains is influenced by both Coulomb forces (the grains are charged) and magnetic forces (grains of superconducting ceramics can be considered equally oriented magnetic dipoles). At this point, the Coulomb forces F_e are inversely proportional to r^2, and the forces of interaction of magnetic dipoles F_m are inversely proportional to r^4[30]:

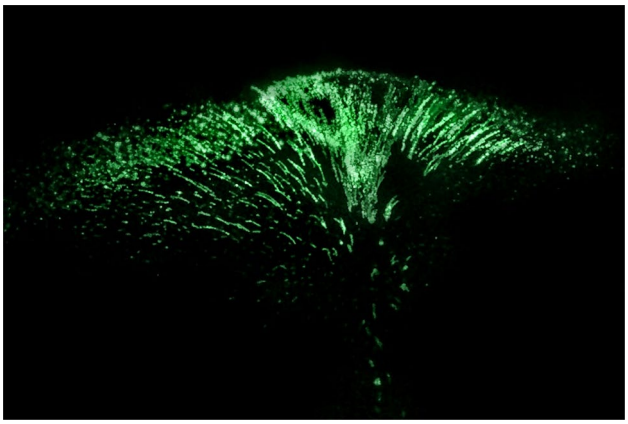

Figure 2. Video frame of a cloud of $YBa_2Cu_3O_7$ grains levitating in superfluid helium. The superconducting ceramic grains are illuminated by laser radiation with a power density $\dot{Q}_p$= 1.9 W/cm^2 (T_{He} = 1.87 K). The structure is illuminated from the right.

Experiment	1	2	3	4
T_{He}, K	1.72	1.87	1.87	1.87
$\dot{Q}_p$, W/cm^2 (% from max power density)	0.3 (20%)	0.7 (40%)	1.3 (70%)	1.9 (100%)
Average grain velocity v_p in a laser beam, mm/s (over the ensemble of moving grains)	0.22	0.52	0.96	1.12
Maximum speed of a single grain, mm/s	1.1	1.2	3.8	3.6
Kinetic energy of grains $E_k = m_p v_p^2/2$ in a laser beam, eV (at $m_p = 2.1 \cdot 10^{-10}$ kg)	$0.32 \cdot 10^2$	$1.8 \cdot 10^2$	$6.1 \cdot 10^2$	$8.3 \cdot 10^2$
Specific entropy loss $\Delta S_k/N_p$, eV/K	$-0.18 \cdot 10^2$	$-0.96 \cdot 10^2$	$-3.3 \cdot 10^2$	$-4.4 \cdot 10^2$

Table 1. The dynamic behavior of grains in the structure under the action of laser radiation of different powers.

$$F_e = \frac{1}{4\pi\varepsilon_o}\frac{Z_p^2}{r^2} \tag{1}$$

and

$$F_m = \frac{3\mu_o p_m^2}{2\pi r^4} \tag{2}$$

Here, $p_m = (\chi_p V_p/\mu_o)B_m$ induced magnetic moment of a grain in a magnetic field with induction B_m, μ_o =1.26·10^{-6} H/m vacuum permeability, χ_p magnetic susceptibility of grain material, and V_p grain volume.

Estimates of these forces for the experimental conditions at φ_p = 20 V, $r \approx d_p$, $\chi_p \approx 0.5$[31], B_m=(10–20)·10^{-3} T yield $Z_p \approx 2.7 \cdot 10^5$ e, p_m=(1.3–2.6)·10^{-10}A·m^2, $F_e \approx 1.1 \cdot 10^{-8}$ N and $F_m \approx$(4.0·10^{-9}–1.6·10^{-8}) N. Note that the condition $F_e \approx F_m \backsim 10^{-8}$ N, which is needed for the formation of chain structures, is met at $Z_p \approx 2.7 \cdot 10^5$ e, p_m=2.6·10^{-10} A·m^2, φ_p = 20 V and B_m=20·10^{-3} T.

Dynamic behavior and spatial structures of grains. Table 1 shows the results of an analysis of the dynamic behavior of grains in the structure at various laser radiation powers in superfluid helium at T_{He} = 1.72 K and 1.87 K, and the corresponding grain structures are shown in Fig. 3 (see also Supplementary Information-Video file "V2.avi"). When estimating, we used the grain with a diameter $d_p \approx 40$ μm and mass $m_p \approx 2.1 \cdot 10^{-10}$ kg, and we analyzed grains in the upper part only (in "umbrella").

One can see from Table 1 that an increase in the power $\dot{Q}_p$ of laser radiation of approximately 2.5 times leads to an increase in the grain kinetic energy $E_k = m_p v_p^2/2$ of approximately 25 times. Note that the grains have an irregular shape (see subplot in Fig. 1a). In addition, we observed random rotation with a characteristic frequency of 50–70 Hz in the experiments.

Thus, there is a mechanism for converting the energy of an external source (laser radiation) into the energy of their kinetic motion, i.e. they are components of an open system, and the motion of the grains themselves can be characterized as the motion of active Brownian grains[7] with strong Coulomb and magnetic interactions. It should be pointed out that such motion can be treated as hot Brownian motion, in accordance with the definition introduced in[32]. The distinctive feature of the motion is the mechanism involving the heating of the grains to a temperature higher than the ambient temperature (the grains are hotter than the environment). Such grains differ

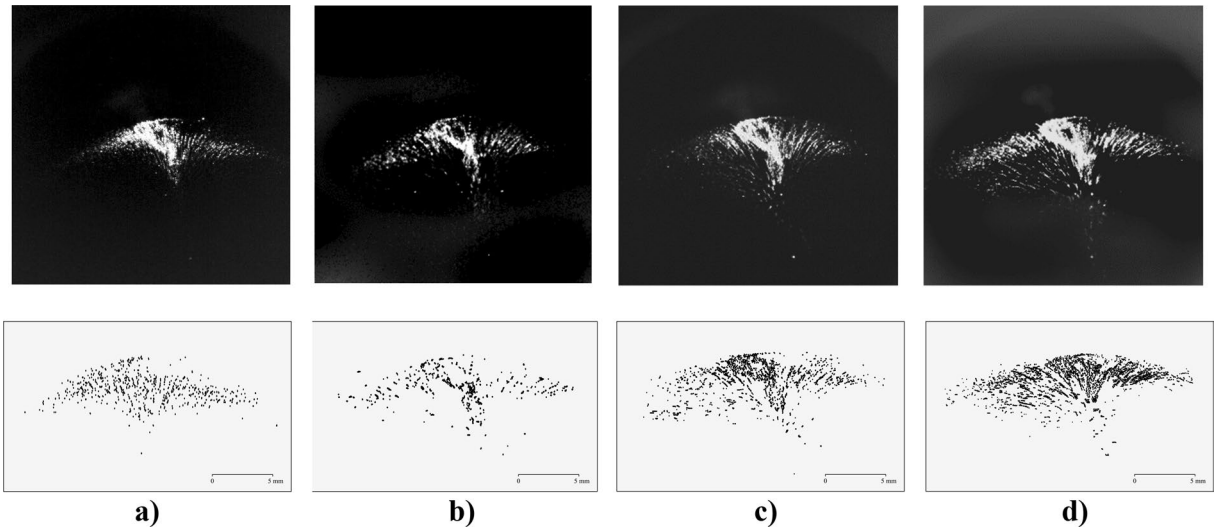

Figure 3. Video frames of a cloud of $YBa_2Cu_3O_7$ grains levitating in superfluid helium and illuminated by laser radiation of various power densities $\dot{Q}_p$. Top row: (**a**) $\dot{Q}_p = 0.3$ W/cm^2 ($T_{He} = 1.72$ K); (**b**) $\dot{Q}_p = 0.7$ W/cm^2 ($T_{He} = 1.87$ K); (**c**) $\dot{Q}_p = 1.3$ W/cm^2 ($T_{He} = 1.87$ K) and (**d**) $\dot{Q}_p = 1.9$ W/cm^2 ($T_{He} = 1.87$ K). Bottom row: the trajectories of grains motion during 0.1 s. The structure is illuminated from the left.

Experiment	1	2	3	4
T_{He}, K	1.72	1.87	1.87	1.87
$\dot{Q}_p$, W/cm^2 (% from max power density)	0.3 (20%)	0.7 (40%)	1.3 (70%)	1.9 (100%)
Number of observed grains	880	683	1010	1354
Total number of grains in chains	252	212	465	728
Total number of single grains	628	471	545	626
Total number of chains, units	52	38	80	98
Fraction of grains in chains, %	29%	31%	46%	54%
Total length of chains, mm	12	14.4	31.6	49.5
Average chain length, mm	0.230	0.380	0.400	0.500
Maximum chain length, mm	0.73	0.88	1.21	1.35
Number of grains in a chain	12	13	18	20
Maximum chain speed, mm/sec	0.56	1.8	2.4	3.2
Number of grains in a chain	4	5	10	12

Table 2. The spatial structures of grains under the action of laser radiation of different powers.

from passive Brownian grains[33], in which the mechanism of grain motion is associated with thermal fluctuations in the surrounding fluid, and the diffusion coefficient D_p is determined by the Einstein formula[34]:

$$D_p = \frac{k_B T_{He}}{6\pi (d_p/2)\eta_n} \tag{3}$$

where k_B—Boltzmann's constant, T_{He}—temperature of the liquid, η_n—viscosity of the liquid, d_p—grain diameter.

The results of our observations also show that with an increase in the laser radiation power density $\dot{Q}_p$, there is not only an increase in the average kinetic energy of grains but also a change in the spatial structures of grains: an increase in the number of chains and their length, while the relative number of single grains decreases (see Table 2 and Fig. 4). Note that with an increase in the value of $\dot{Q}_p$, the number of observed (visible) grains also increases, which can be explained by the threshold nature of their video recording (a grain can be observed if the scattering of laser radiation on it exceeds a certain threshold of video camera sensitivity).

Brownian motion of grains. To analyze the Brownian motion of single grains, as well as grains within the chains, we calculated the experimental time dependences of their mean-square displacement (MSD) $< \Delta r^2(t) >$ for various powers of laser illumination (see Fig. 5). The figure plotted in log–log scale shows straight lines corresponding to different modes of Brownian motion MSD $\sim t^{\beta}$[35–37]: ballistic motion ($\beta = 2$), anomalous diffusion

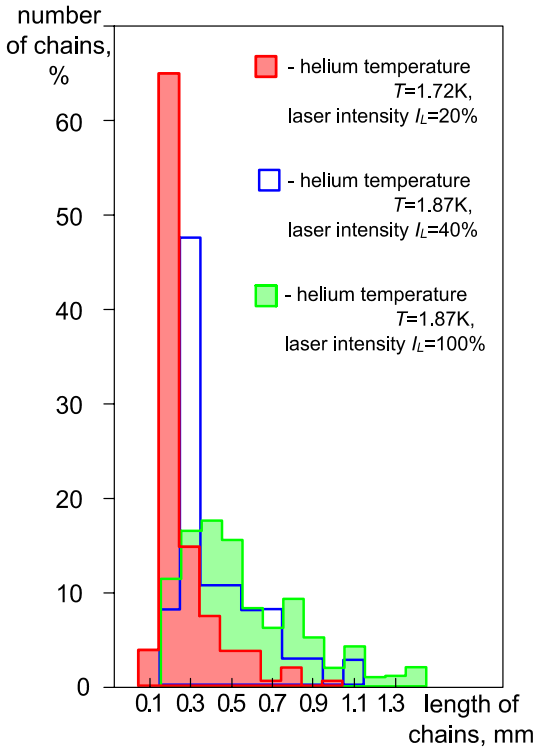

Figure 4. Distribution of chains by lengths in the structure under the action of laser illumination of various power densities $\dot{Q}_p$: red indicates $\dot{Q}_p = 0.3$ W/cm^2 ($T_{He} = 1.72$ K); blue presents $\dot{Q}_p = 0.7$ W/cm^2 ($T_{He} = 1.87$ K) and green is for $\dot{Q}_p = 1.9$ W/cm^2 ($T_{He} = 1.87$ K).

$(3/2 < \beta < 2)$ and normal diffusion ($\beta = 1$). The characteristic trajectories of motion of single grains in the structure are shown in the inset in Fig. 5. Note that theoretically, the problem of the Brownian motion of a grain in superfluid helium was considered in a number of works[38–42].

In our experiments, under the action of laser radiation, a change in MSD is observed at characteristic times $\tau \approx 0.02$–1.0 s; at longer times ($\tau \geq 0.7$ s). Brownian motion was diffusive with the following diffusion coefficients: $D_p \approx 6.0 \cdot 10^{-8}$ m^2/s (at $T_{He} = 1.72$ K and $\dot{Q}_p$=0.3 W/cm^2) and $D_p \approx 3.3 \cdot 10^{-7}$ m^2/s (at $T_{He} = 1.87$ K and $\dot{Q}_p$=1.9 W/cm^2). From Einstein's formula (3), the following values of the diffusion coefficients can be obtained: $D_{He} \approx 4.9 \cdot 10^{-14}$ m^2/s ($T_{He} = 1.72$ K and $\eta_n = 1.29 \cdot 10^{-6}$ Pa·s[43]) and $D_{He} \approx 5.2 \cdot 10^{-14}$ m^2/s ($T_{He} = 1.87$ K and $\eta_n = 1.32 \cdot 10^{-6}$ Pa·s[43]), which are less than those obtained from experiments, by 6–7 orders of magnitude.

For short times $(0.02 \leq \tau \leq 0.7$ c), grain diffusion is abnormal, $< \Delta r^2(t) > \sim t^{\beta}$, where $1 < \beta < 3/2$ (superdiffusion)[1,35–37].

The experimentally obtained values of the diffusion coefficients agree by order of magnitude with those calculated from formula (3) at $k_B T \approx E_k = m_p v_p^2/2$: $D_p \approx 1.0 \cdot 10^{-8}$ m^2/s ($E_k \approx 0.32 \cdot 10^2$ eV at $T_{He} = 1.72$ K and $\dot{Q}_p$ =0.34 W/cm^2) and $D_p \approx 2.7 \cdot 10^{-7}$ m^2/s ($E_k \approx 8.3 \cdot 10^2$ eV at $T_{He} = 1.87$ K and $\dot{Q}_p$=1.9 W/cm^2).

For the Brownian motion of grains in a classical liquid (non quantum), the ballistic regime ($< \Delta r^2(t) > \sim t^2$) takes place at times[44–46] $\tau \leq m_p/(6\pi (d_p/2)\eta_n) \approx 0.4$ s (at $T_{He} = 1.72$ K and $T_{He} = 1.87$ K), whereas in our case, grains' motion is not ballistic even at $\tau \approx 0.02$–0.4 s (see Fig. 5).

Note that the Brownian motion of grains within chains is characterized by the localization of their motion. As a result, the time dependence of the mean-square displacement of grains in the chain has the form of a plateau (see Fig. 5).

The relative contribution of directed grain motion in comparison with random motion at temperature T_{He} can be characterized by the Peclet number[47]:

$$Pe = \frac{d_p v_p}{D_{He}} \tag{4}$$

At $D_p \approx 4.9 \cdot 10^{-14}$ m^2/s ($T_{He} = 1.72$ K and $\dot{Q}_p$=0.3 W/cm^2) and $D_p \approx 5.2 \cdot 10^{-14}$ m^2/s ($T_{He} = 1.87$ K and $\dot{Q}_p$=1.9 W/cm^2), Eq. (4) yields $Pe \sim 1.8 \cdot 10^5$ and $Pe \sim 8.6 \cdot 10^5$, correspondingly. Thus, the intensity of the motion of chains and single grains increases with an increase in the power of laser radiation.

We also gradually reduced the intensity of laser beam radiation acting on the structure of grains to zero, then switched on the laser again and increased the power of its radiation within 3 s to ~5% of the maximum value, after which we measured grains' speed. The average velocity was $v_p \sim 0.12$ mm/s (at $T_{He} = 1.87$ K), which corresponds to kinetic energy $E_k = m_p v_p^2/2 \approx 9.5$ eV. At helium temperature T_{He}, the kinetic energy of the grains should have a value of $\sim k_B T_{He} \approx 1.6 \cdot 10^{-4}$ eV.

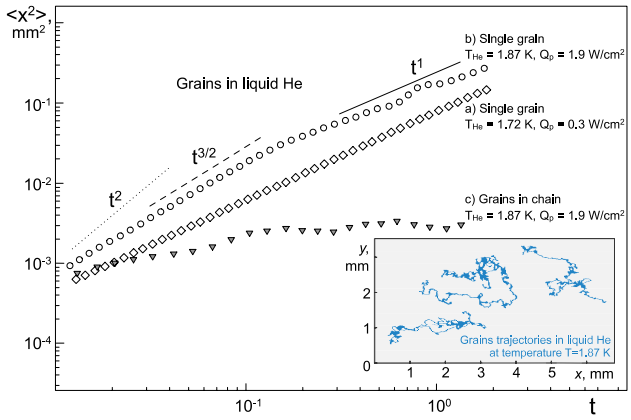

Figure 5. Mean-square displacements of grains in the structure under the action of laser illumination of various power densities $\dot{Q}_p$: (**a**) single grain at $\dot{Q}_p = 0.3$ W/cm^2 ($T_{He} = 1.72$ K); (**b**) single grain at $\dot{Q}_p = 1.9$ W/cm^2 ($T_{He} = 1.87$ K) and (**c**) grains within chain at $\dot{Q}_p = 1.9$ W/cm^2 ($T_{He} = 1.87$ K). The inset shows the characteristic trajectories of grains.

Evolutionary process of Brownian grains. Thus, the observed systems of active Brownian grains in superfluid helium can be considered as open systems (there is an exchange of energy with the environment), and the ordered structures of grains are the structures far from equilibrium. Such structures are called dissipative; in these structures, the scattering of the energy coming from outside makes possible a stationary ordered structure with an entropy less than the equilibrium one. In dissipative structures, a change (increase) in the flow of entropy into the environment can occur, which results in their self-organization and evolution[1–4].

Self-organization and evolution of open systems at all levels occurs due to the outflow of entropy into the environment, while the free energy entering a stationary system should exceed the contribution from the production of entropy in the system[1,2]. In our experiments, grains of superconducting ceramics in superfluid helium obtain energy $\dot{Q}_p$ when from laser radiation with an effective temperature T_L, which can be calculated from the following relation[48]:

$$\dot{Q}_p = \Delta\lambda\left(\frac{2\pi hc^2}{\lambda^5}\right)\frac{1}{e^{hc/\lambda k_B T_L} - 1}, \tag{5}$$

Therefore, for T_L, we can write:

$$T_L = hc/\lambda k_B\left[ln\left(1 + \Delta\lambda\left(\frac{2\pi hc^2}{\lambda^5}\right)\frac{1}{\dot{Q}_p}\right)\right]^{-1} \tag{6}$$

Here, h—Planck constant, c–light speed, $\lambda = 532$ nm—laser radiation wavelength, and $\Delta\lambda$—laser radiation line width. Given that $\dot{Q}_p = 0.26$–1.9 W/cm^2 and $\Delta\lambda \approx 1$ nm, we find that T_L is in the range $(3.3–4.4)\cdot 10^3$ K, which is much higher than the temperature of superfluid helium T_{He}.

Due to the thermal balance in the system, the grains transfer exactly the same amount of energy to superfluid helium. Due to the thermodynamic relation $\delta Q = TdS$, the total export of entropy is equal to[1,2]:

$$\frac{dS_p}{dt} = \dot{Q}_p\left[\frac{1}{T_L} - \frac{1}{T_{He}}\right] < 0 \tag{7}$$

At $T_{He} = 1.87$ K and $\dot{Q}_p = 0.26$–1.9 W/cm^2 entropy export density $\frac{dS_p}{dt}$ is in the range

$$\frac{dS_p}{dt} = -(0.14 - 1.02)\text{W/Kcm}^2 \tag{8}$$

In dissipative structures, part of the decrease in entropy ΔS_k of the system, as opposed to the equilibrium case, is due to the kinetic energy E_k of moving grains[49]:

$$\Delta S_k = -\frac{E_k}{T_{He}} = -\frac{N_p\left(\frac{m_p v_p^2}{2}\right)}{T_{He}}, \tag{9}$$

where N_p is the number of observed grains in the laser beam.

The calculations of the specific (per grain) entropy loss $\Delta S_k/N_p$ at $T_{He} = 1.87$ K, presented in Table 1, show a significant increase in $|\Delta S_k/N_p|$ in the system of grains (by approximately two orders of magnitude) with an increase in the laser radiation intensity from 0.26 to 1.9 W/cm^2.

Thus, an increase in the power of laser radiation leads to an increase in the kinetic energy of grains and chains, and we observe a growth in the number of ordered and stable autonomous structures (chains) of grains in the levitating cloud as well. Laser radiation also induces the transition of a strongly nonequilibrium stationary system of ceramic grains to a state with a lower entropy (evolution process), i.e. into a more ordered state.

Grain motion and quantum turbulence. It is a common fact that the motion of grains in superfluid helium can be quite complex[12]. The normal liquid ^{4}He (He I), when cooled below $T_\lambda = 2.177$ K (λ-point), undergoes a second-order phase transition; the low-temperature phase is known as He II[49]. The physical properties of He II cannot be described by classical physics; it is a quantum liquid exhibiting unusual physical properties such as superfluidity[11]. Phenomenologically, He II is described by a two-fluid model[50], in which it consists of two components: a viscous normal fluid with a density ρ_n, which carries all the entropy, and a non viscous superfluid component with a density ρ_s; the total density of He II is $\rho = \rho_n + \rho_s$. At T_λ and higher, helium is a normal liquid, while at the limit of zero temperature, there is no normal liquid. For many practical purposes, He II can be considered as consisted only of a superfluid component at temperatures below 1 K.

The superfluid component has a temperature-dependent density $\rho_s(T)$ and is 100% of the total fluid density ρ at absolute zero ($\rho_s(T=0) = \rho$). It has no viscosity and no entropy; on the other hand, a normal fluid (with density $\rho_n(T = T_\lambda) = \rho$) behaves in the same way as a classical fluid.

Under certain conditions, quantum turbulence occurs in He II, and its circulation is limited by quantized vortex lines, each of which has a quantum of circulation $\kappa \approx 10^{-7}$ m^2/s around the core, with a diameter of approximately $\xi_o \approx 0.1$ nm[51,52]. It was first considered in the work of Feynman[53], while in a thermally induced flow of He II created by an electric heater, it was experimentally studied and theoretically described by Vinen[52,54–57]. In the presence of a heat source, a normal fluid carries entropy away from the source with a velocity v_n, while a superfluid liquid moves to the heat source with a velocity v_n so that the total mass flow rate is zero, $\rho_n v_n + \rho_s v_s = 0$[58]. Thus, a thermal counterflow is created, the relative velocity $v_{ns} = |v_n| + |v_s|$ of which is proportional to the applied heat flow $\dot{Q}$. It should be noted that the interaction of the normal component with quantized vortices generates nonclassical forces of mutual friction[54–57].

The normal fluid velocity relates to the magnitude of the heat flux $\dot{Q}$ as[12]:

$$v_n = \frac{\dot{Q}}{\rho S_n T_{He}}, \tag{10}$$

and to the relative velocity of the counterflow as[12]:

$$v_{ns} = \frac{\dot{Q}}{\rho_s S_n T_{He}}, \tag{11}$$

where S_n is the specific entropy of the normal component.

When the heat flux increases, the counterflow velocity v_{ns} also increases, and turbulence can develop in both components of the liquid[58,59] when the critical value exceeds $v_{ns}^0 \sim 2$ mm/s[59–61]. The critical value of the heat power density is $\dot{Q}_{cr} \sim 20$ mW/cm^2[59,60].

Superfluid turbulence manifests itself in the form of a quantized vortex tangle[12,59,61,62], the density L of which is determined by the relation:

$$L = \gamma^2 (v_{ns} - v_{ns}^0)^2 = \gamma^2 \left(\frac{\dot{Q}}{\rho_s S_n T_{He}} \right)^2 \tag{12}$$

where γ is a temperature-dependent parameter[62–64].

When laser radiation acts on the surface of a ceramic grain, it generates a local heat release, which should cause the movement of the normal component from the grain and the superfluid component to the grain. In our experiments at $T_{He} = 1.72$ K ($S_n = 3.95 \cdot 10^2$ J/(kg·K), $\rho = 1.45 \cdot 10^2$ kg/m^3, $\rho_s = 1.12 \cdot 10^2$ kg/m^3[43]) and heat release power density $\dot{Q} = \dot{Q}_p = 0.26$–$1.9$ W/cm^2, the velocity of the normal component is in the range of 1.7–12.2 cm/s, and the relative counterflow velocity v_{ns} is in the range of 2.1–15.8 cm/s. At $T_{He} = 1.87$ K ($S_n = 6.27 \cdot 10^2$ J/(kg K), $\rho = 1.45 \cdot 10^2$ kg/m^3, $\rho_s = 0.925 \cdot 10^2$ kg/m^3[43]) and the same power density of heat release, the velocity of the normal component is in the range of 1.5–11.2 cm/s, and the relative counterflow velocity v_{ns} is in the range of 2.4–17.5 cm/s. This means that $v_{ns} >> v_{ns}^o$.

Thus, the action of laser radiation on grains should lead to the formation of quantum vortices near the grain surface. Such a method of the formation of quantum vortices (their generation by grains during laser heating, in which the grains act as "point" heaters) is fundamentally different from the well-known works in which grains act as vortex markers[59,65].

As a result, a variety of effects associated with quantum turbulence can arise in such a system. For example, when quantum vortices collide with the grain surface and transfer their momentum to the grain[66], they can be whirled away by the superfluid component moving in the direction of the laser beam to the heated surface of the ceramic grain. The force F_s acting on a grain when interacting with a superfluid component is determined by the relation[12,62]:

$$F_s \approx \frac{\rho_s \kappa^2}{4\pi} 2\beta_d \left(\frac{d_p/2}{\ell} \right)^2 \ln \frac{(d_p/2)}{\xi_0} \tag{13}$$

Experiment	1	2	3	4
T_{He}	1.72 K	1.87 K	1.87 K	1.87 K
$\dot{Q}_p$, W/cm^2	0.3 (20%)	0.7 (40%)	1.3 (70%)	1.9 (100%)
Quantum vortex density L, 10^{10} m^{-2}	0.81	1.9	5.8	12.3
Mean distance between vortices ℓ, μm	11.1	7.3	4.1	2.9
Average grain speed, mm/s	0.22	0.52	0.96	1.12
Average grain acceleration, mm/s^2 (over the ensemble of moving grains)	21	–	–	320
Kinetic energy of grains $E_k = m_p v_p^2/2$ in a laser beam, eV (at $m_p = 2.1{\cdot}10^{-10}$ kg)	$0.32{\cdot}10^2$	$1.8{\cdot}10^2$	$6.1{\cdot}10^2$	$8.3{\cdot}10^2$
Diffusion coefficients: D_p, m^2/s	$6.0{\cdot}10^{-8}$			$3.3{\cdot}10^{-7}$
Resultant force F_Σ, 10^{-11} N	0.44	–	–	6.8
Work done by $F_\Sigma : A_\Sigma \sim F_\Sigma d_p$, eV	$1.1{\cdot}10^3$	–	–	$1.7{\cdot}10^4$
Specific entropy loss, $\Delta S_\Sigma/N_p$, eV/K	$0.64{\cdot}10^3$	–	–	$0.9{\cdot}10^4$
Force F_s , 10^{-11} N	0.7	1.4	4.2	8.9
Work done by $F_s : A_s \sim F_s d_p \sim E_V$, eV	$1.7{\cdot}10^3$	$3.5{\cdot}10^3$	$1.0{\cdot}10^4$	$2.2{\cdot}10^4$
Specific entropy loss, $\Delta S_s/N_p$, eV/K	$-1.0{\cdot}10^3$	$-1.87{\cdot}10^3$	$-5.6{\cdot}10^3$	$-1.2{\cdot}10^4$
Force F_n, 10^{-11} N	0.011	0.026	0.048	0.056
Force F_r , 10^{-10} N	0.65	2.0	6.23	13.1

Table 3. The averaged forces F_Σ, F_s, F_n and F_r for grains in the structure, obtained from experimental data on the velocities of ceramic grains.

where β_d is the geometric factor of the order of unity ($\beta_d \approx 1$), $\ell = L^{-1/2}$ is the average distance between vortices and $((d_p/2)/\ell)^2$ is a cross section of the interaction of a grain with a system of quantum vortices. When deriving relation (13), it was assumed that $(d_p/2) >> \ell$[12,62].

For comparison, we also estimate the force F_r, which can arise during momentum transfer to a grain by the normal component. This is the case for a potential (vortex-free) helium flow when the superfluid component transforms into a normal liquid to carry away heat from the grain surface[67]:

$$F_r \approx \frac{\dot{Q}}{S_n T_{He}} \pi (d_p/2)^2 v_s = \left(\frac{\dot{Q}}{S_n T_{He}}\right)^2 \pi (d_p/2)^2 \frac{\rho_n}{\rho_s \rho} \tag{14}$$

Let us estimate the force F_n of the normal component acting on a ceramic grain moving with a velocity v_p at different laser radiation powers using the Stokes law[12]:

$$F_n = 6\pi (d_p/2) \eta_n v_p \tag{15}$$

where η_n viscosity of the normal component of helium.

The energy E_V stored in a vortex tangle near the grain surface can be estimated as

$$E_V \sim d_p^3 L E_{QT} \sim d_p^3 L \frac{\rho_s \kappa^2}{4\pi} \ln \frac{(d_p/2)}{\xi_0} \sim F_s d_p \sim A_s \tag{16}$$

where $E_{QT} = \frac{\rho_s \kappa^2}{4\pi} \ln \frac{(d_p/2)}{\xi_0}$ is the energy per unit length of the quantum vortex and $A_s \sim F_s d_p$ is the characteristic work done by force F_s.

The results of estimates of the averaged forces F_n, F_s and F_r for grains in the structure, obtained from experimental data on the velocities of ceramic grains at $T_{He} = 1.72$ K ($\eta_n = 1.29{\cdot}10^{-6}$ Pa·s) and $T_{He} = 1.87$ K ($\eta_n = 1.32{\cdot}10^{-6}$ Pa·s) are presented in Table 3 at different powers of laser radiation. The density of quantum vortices at different powers of laser radiation is estimated by formula (12) at $\gamma \approx 200$ s/cm^2[64] and $\beta_d \sim 1$[12,62].

The table also shows the resulting force F_Σ acting on the grain and estimates of the characteristic work $A_\Sigma \sim F_\Sigma d_p$ and $A_s \sim F_s d_p$ done by forces F_Σ and F_s. The forces $F_\Sigma = m_p a_p$ (at $m_p = 2.1{\cdot}10^{-10}$ kg) are obtained from experimental data on the accelerations a_p of grains moving in superfluid helium. Table 3 also presents estimates of the decrease in entropy in the system of grains, corresponding to the work done by the forces F_Σ and F_s[68].

We can also evaluate a light pressure force F_{ph} acting on grain when the grain is illuminated by laser radiation with heat release power density $\dot{Q}_p$ on the surface of the grains[69]:

$$F_{ph} \approx \frac{2\dot{Q}}{c} \pi (d_p/2)^2, \tag{17}$$

where c is the velocity of light in a vacuum.

In our experiments at $\dot{Q}_p \approx 2$ W/cm^2, the force F_{ph} is approximately $4{\cdot}10^{-14}$ N. This value is less than the forces F_Σ, F_s, F_n and F_r by 2–4 orders of magnitude. Thus, the light pressure force does not have a significant effect on the dynamics of the grain motion and can be neglected.

The thermophoresis forces associated with the temperature gradient in superfluid helium near the surface of the grain[70] can be ignored: as follows from[71], the temperature jump in superfluid helium over grain size $d_p \approx 40$ μm is negligibly small (less than 1 mK).

The results of estimates performed with an accuracy of an order of magnitude (see Table 3) show that $F_\Sigma \backsim F_s$ and $A_\Sigma \sim A_s \sim E_V \gtrsim E_k$, while the specific entropy $\Delta S_s/N_p$ is approximately two orders of magnitude higher than the specific entropy $\Delta S_k/N_p$. This means that specific entropy loss can be characterized not only by the kinetic motion of ceramic grains but also by the formation of quantum vortices near their surface when the grains are heated by laser radiation.

Quantum effects in Brownian motion, evolution and interaction of grains. The development of quantum turbulence and the formation of quantum vortices near the grain surface, when they are heated by laser radiation, also has a driving effect on the motion of grains in superfluid helium. In this case, the role of thermal fluctuations in the density of the medium can be played by fluctuations in the density of quantum vortices ΔL, which can have a value of $\Delta L \sim 0.01$[72], which corresponds to energy fluctuations $\Delta E_V \sim 0.01 E_V \sim 0.01 A_\Sigma \sim 10^2$ eV (see Table 3). Note that $\Delta E_V \sim E_k$ by an order of magnitude (see also Table 1), which is in favor of the above mentioned assumption. The characteristic times of the ballistic motion of grains can be estimated as $\tau \sim \ell/v_p = L^{-1/2}/v_p \sim 10^{-3}$–$10^{-2}$ s at $\ell \sim 1$–10 μm and $v_p \sim 0.1$–1.0 mm/s.

In the experiments, the action of the laser radiation can lead to the nonuniform heating of the grain surface. This is due to inhomogeneous illumination of the surface of single grains when the grain size is much larger than the wavelength of laser radiation (in the approximation of geometric optics)[73]. In addition, the grains have an irregular shape. Thus, their surface is heated unevenly so that the density of quantum vortices varies along the surface (see relation (12)); hence, spontaneous symmetry breaking associated with the space–time change in the density of quantum vortices is observed[74,75]. As a result, the grain gets an uncompensated impulse (see relation (13)), fluctuating in magnitude and direction, and the intensity of Brownian motion of the grain, both translational and rotational, increases.

It should be noted that the grain motion is hot Brownian motion, which, due to spontaneous symmetry breaking, can be treated as active Brownian motion[32].

Such a mechanism of motion of grains can be considered as an experimental implementation of a quantum Brownian motor in a regime where quantum fluctuation effects become significant for the transport properties[76,77].

Thus, an increase in the kinetic energy in a system of grains and an increase in the energy of quantum vortices (and thus a decrease in entropy in the system) is due to the mechanism of heat loss from the surface of grains by the normal component of helium, including the formation of quantum vortices (quantum turbulence). In this case, relation (7) can be transformed to the form:

$$\frac{dS_p}{dt} = \dot{Q}_p \left[\frac{1}{T_L} - \frac{1}{T_{He}} \right] \approx -\frac{\dot{Q}_p}{T_{He}} = -v_n \rho S_n < 0 \tag{18}$$

We assume that laser radiation induces a transition (evolution) of a stationary system of ceramic grains far from equilibrium to a more ordered state (which is also a stationary state far from equilibrium), i.e. into a state with less entropy. Note that a negative entropy flux in a cloud of macroscopic grains (which leads to a decrease in entropy in the system) is created by a kind of quantum entropic pump[78], whose work consists of entropy loss from the system by the normal component of superfluid helium with a speed $v_n \lesssim 10.0$ mm/s, at this $\frac{dS_p}{dt} \backsim 10^4$ W/(m^{2}K).

Above the λ-point, the thermal conductivity of liquid helium has the value $\kappa \backsim 2.0 \cdot 10^{-2}$ W/(m·K), so we can estimate the following:

$$\frac{dS_p}{dt} \approx -\frac{\dot{Q}_p}{T_{He}} = -\kappa \frac{\Delta T}{\Delta r} \frac{1}{T_{He}} \tag{19}$$

At $\Delta T \approx 1$ K, $\Delta r \approx d_p \approx 4 \cdot 10^{-5}$ m, we obtain $\frac{dS_p}{dt} \backsim 10^2$ W/(m^{2}K), which is much less (by 1.5—2 orders of magnitude) than the above estimate for the conditions of superfluid helium.

When crossing the λ-point, the character of grain motion changes qualitatively: grains are carried out by the ascending convective flow from the overheated zone (see Fig. 6 and Supplementary InformationVideo file "V3.avi"). The grain velocity in this case is on the order of 1 m/s, since we did not detect grains upstream that were sequentially recorded for at least 2 frames of the video recording (at a frame rate of 200 frames/s). The height of the observation area above the structure is approximately 5 mm, which gives an estimate of the minimum speed of 1 m/s.

In superfluid helium, the density of quantum vortices depends quadratically on the power density of laser radiation. The size of the region in which quantum vortex tangles occur is also proportional to laser radiation. To estimate the characteristic dimension of the region of quantum turbulence, we use the relation[79]:

$$v_n 4\pi r^2 \rho S_n = \frac{I_L}{T_{He}} \tag{20}$$

We assume that the threshold power density of thermal radiation for the formation of quantum turbulence on the surface of a grain with a diameter of $d_p = 40$ μm is $\dot{Q}_{cr} = 20$ mW/cm^2. Then, an increase in the power density of heat release under the action of laser radiation on the grain surface up to values $\dot{Q}_p = 0.26$–1.9 W/cm^2 increases the size of the D_{QT} region of quantum turbulence up to values $D_{QT} = d_p(\dot{Q}_p/\dot{Q}_{cr})^{1/2} \sim (4$–$10) d_p \approx 160$–$400$ μm.

The spatial picture of quantum vortices and grains captured by them is schematically shown in Fig. 7. Note that the charge of the grains in the experiment remained unchanged, and the magnetic moment of the grains depends only on the spatial position (the magnetic field is inhomogeneous, see Fig. 1b).

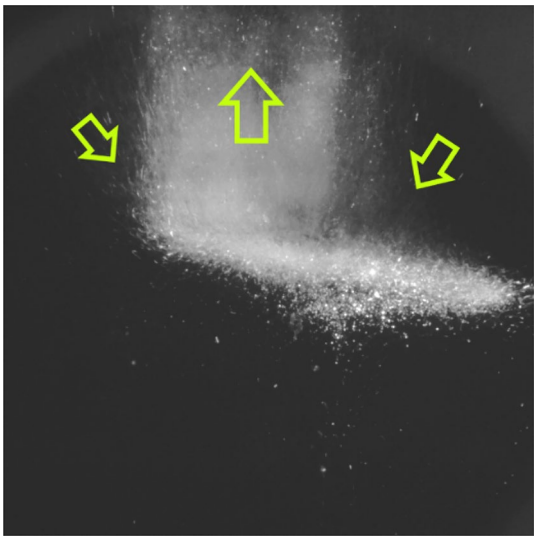

Figure 6. Processes in a structure exposed to laser radiation at $T = 2.17$ K. Video frame of a cloud of superconducting ceramic grains levitating in superfluid helium, carried away by an ascending convective flow from the overheated zone. The direction of motion of the grains is shown by arrows. The structure is illuminated from the left.

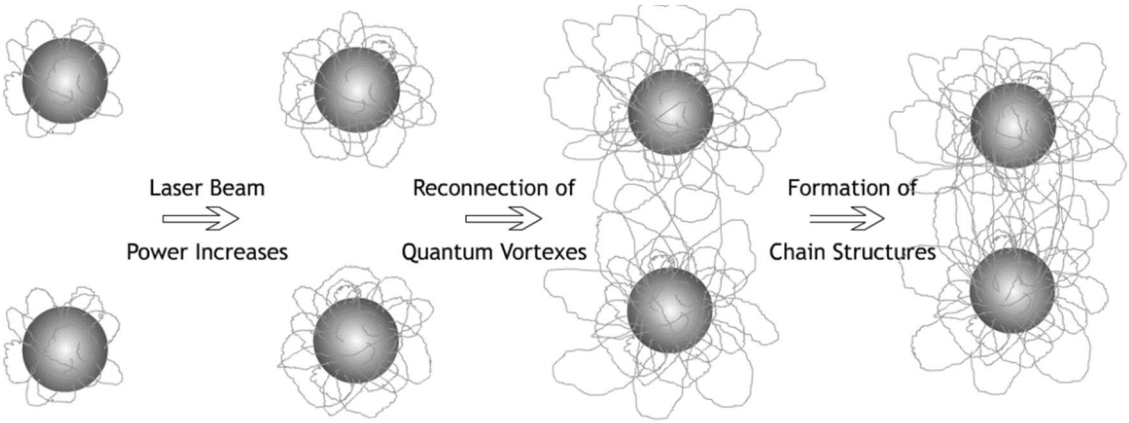

Figure 7. Schematic illustration of the spatial picture of quantum vortices and grains captured by them.

Such a density growth of quantum vortices increases the effective cross section for the interaction of two grains with the value $\sim D_{QT}^2 \sim d_p^2(\dot{Q}_p/\dot{Q}_{cr})$ due to the overlap of vortices' tangle and their reconnection (see Fig. 7) and thus increases the probability of capture of the nearest grains and their subsequent confinement into chain structures. The characteristic volume of grain capture per unit time is $\sim D_{QT}^2 v_p \sim d_p^2(\dot{Q}_p/\dot{Q}_{cr})v_p$ and can increase by approximately 30 times with a change in the heat release of laser power $\dot{Q}_p$ from 0.26 W/cm^2 to 1.9 W/cm^2. Since the energy of a quantum vortex depends on the length of the chain and it is energetically favorable for it to decrease its length[12], a tension force arises, which can pull grains or chains together, resulting in an increase in the number of chains and their length[62]. This is confirmed by the estimates given in Table 3, which show that $A_s \backsim E_V \gtrsim E_k$.

Let us estimate the characteristic binding energy E_b of grains in a chain. For this, we use the results of experimental observation of the formation of a chain due to the collision of a chain moving with a velocity v_p = 2–3 mm/s with a motionless chain confined in the structure (see Fig. 8 and Supplementary InformationVideo file "V4.avi"):

$$E_b \gtrsim E_k \sim \frac{m_p v_p^2}{2} \sim F_e d_p \sim F_m d_p \tag{21}$$

Here, E_k—kinetic energy of the grain in the chain. For v_p =3 mm/s and p_m=1.3·10^{-10} A·m^2 one can see that $F_e \sim F_m \sim 2.4 \cdot 10^{-11}$ N at intergrain distance $r_{min} \sim 200$ μm. Note that the obtained values $F_e \sim F_m \sim F_s$, that is why tension forces associated with quantum vortices can make a significant contribution to the trapping of grains during the formation of chains.

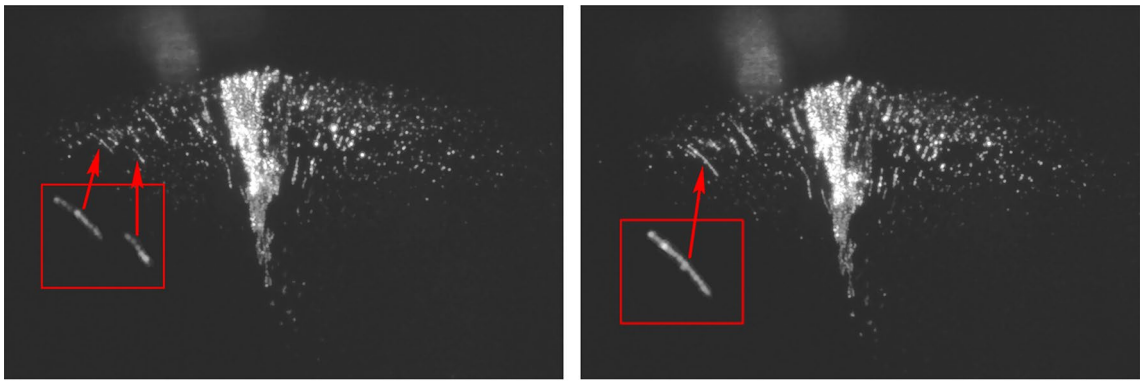

a) b)

Figure 8. Video frames of the chain formation as a result of a collision of two moving fragments at speeds $v_p \approx$ 2–3 mm/s. (**a**) before the collision; (**b**) after the collision. The structure is illuminated from the left.

Note that an estimate of the characteristic binding energy E_b of grains in the chain was also calculated using data from experimental observation of the transition of helium from the normal to the superfluid state. In this case, before the formation of chains, the grains can move at speeds up to 5–6 cm/s. It corresponds to the value $E_b \backsim 4.7 \cdot 10^6$ eV, which is in good agreement (by the order of magnitude) with the energy of grain trapping in the chain by the forces $F_e \approx F_m \backsim 10^{-8}$ N, which in turn is comparable with work done by these forces $A_e \sim F_e d_p \sim A_m \sim F_m d_p \sim 2.5 \cdot 10^6$ eV.

Conclusions

We present the results of a study of the Brownian motion of grains of superconducting ceramics with sizes up to 60 μm and electric charges up to 10^5 *e* levitating in a static magnetic trap in superfluid helium (cryogenic colloid) at temperatures of 1.7–2.18 K under the action of laser radiation with a power density of up to ~ 2 W/cm^2. It is revealed that growth of the power density of laser radiation increases the kinetic energy of the motion of grains and their diffusion coefficient by 6–7 orders of magnitude compared to equilibrium values at temperatures of superfluid helium. It is shown that the motion of grains can be regarded as a motion of active Brownian grains with strong Coulomb and magnetic interactions.

The active Brownian motion of grains in superfluid helium under experimental conditions (at temperatures below the λ-point) is associated with the interaction of the normal and superfluid components of He with the grain surface and with each other due to the appearance of a quantum vortex tangle when the grain surface is heated by laser radiation. The nature of the macroscopic motion of grains changes drastically when helium transits into the normal state, and the grains are carried away by the convection flow of heated helium into the field of gravity. Thus, this active Brownian macroscopic motion is associated with quantum turbulence.

It is also shown that an increase in the laser radiation, when it acts on a cloud of grains, induces the self-organization and evolution of the grain's system, with the transitions of the system to a more complex state with a lower entropy, while the negative flux of entropy in the system is created due to the quantum mechanism of exceedingly high entropy loss in superfluid helium, associated with the transfer of heat by the normal component of superfluid helium, with the formation of quantum vortices. The most unexpected outcome here is the increase in the number and length of grain chains with the increase in the power density of laser radiation.

Thus, grain structures in our experiments in superfluid helium can be considered dissipative structures, that is, stationary systems far from equilibrium, in which active Brownian motion, as well as the evolution of structures, were driven by quantum effects.

Received: 30 November 2021; Accepted: 23 March 2022
Published online: 12 April 2022

References

1. Ebeling, W., Engel, A. & Feistel, R. *Physik Der Evolutionsprozesse* (Akademie-Verlag, 1990).
2. Ebeling, W. & Feistel, R. *Physics of Self-Organization and Evolution* (Wiley-VCH, 2011).
3. Prigogine, I. *Introduction to Thermodynamics of Irreversible Processes* (Charles C Thomas Publisher, 1955).
4. Prigogine, I., Nicolis, G. & Babloyantz, A. Thermodynamics of evolution. *Phys. Today* **25**(11), 23–28 (1972).
5. Schrodinger, E. *What is Life? The physical aspect of the living cell. Based on lectures delivered under the auspices of the Dublin Institute for Advanced Studies at Trinity College* (Dublin, 1943).
6. Zwicker, D., Seyboldt, R., Weber, C., Hyman, A. A. & Jülicher, F. Growth and division of active droplets provides a model for protocells. *Nat. Phys.* **13**, 408–413 (2017).
7. Bechinger, C. *et al.* Active particles in complex and crowded environments. *Rev. Mod. Phys.* **88**, 045006 (2016).
8. Vasiliev, M. M., Petrov, O. F. & Statsenko, K. B. Coulomb structures of charged macroparticles in static magnetic traps at cryogenic temperatures. *JETP Lett.* **102**, 771–774 (2015).
9. Vasilieva, E. V., Petrov, O. F. & Vasiliev, M. M. Laser-induced melting of two-dimensional dusty plasma system in RF discharge. *Sci. Rep.* **11**, 523 (2021).

10. Fröwis, F., Sekatski, P., Dür, W., Gisin, N. & Sangouard, N. Macroscopic quantum states: Measures, fragility, and implementations. *Rev. Mod. Phys.* **90**, 025004 (2018).
11. Kapitza, P. Viscosity of liquid helium below the λ-point. *Nature* **141**, 74 (1938).
12. Barenghi, C. F. & Sergeev, Y. A. (eds) *Vortices and Turbulence at Very Low Temperatures International Centre for Mechanical Sciences Courses and Lectures* (Springer, 2008).
13. Inui, S. & Tsubota, M. Spherically symmetric formation of localized vortex tangle around a heat source in superfluid He 4. *Phys. Rev. B* **101**, 2 (2020).
14. Thomson, W. *Reprint of papers on electrostatics and magnetism*. paper XXXIII, pp. 493–499, and paper XXXIV, pp. 514–515 (MacMillan, London, 1872).
15. Braunbek, W. Freischwebende Ko¨rper im elecktrischen und magnetischen Feld. *Z. Phys.* **112**, 753–763 (1939).
16. Savin, S. F., Dyachkov, L. G., Vasiliev, M. M., Petrov, O. F. & Fortov, V. E. Clusters of charged diamagnetic particles levitating in nonuniform magnetic field. *EPL* **88**, 64002 (2009).
17. Savin, S. F. *et al.* Coulomb ensemble of charged diamagnetic macroparticles in an inhomogeneous magnetic field under microgravity conditions. *JETP Lett.* **94**, 508–512 (2011).
18. Petrov, O. F. *et al.* Coulomb clusters of dust particles in a cusp magnetic trap under microgravity conditions. *Phys. Rev. E.* **86**, 036404 (2012).
19. Parfenov, V. A. *et al.* Magnetic levitational bioassembly of 3D tissue construct in space. *Sci. Adv.* **6**, 4174 (2020).
20. Bednorz, J. G. & Muller, K. A. Possible high-TC superconductivity in the Ba-La-Cu-O system. *Zeitschrift fur physik b-condensed matte* **64**, 189–193 (1986).
21. Meissner, W. & Ochsenfeld, R. Ein neuer Effekt bei Einfritt der Supraleitfaihigkeit. *Naturwissenschaften* **21**(44), 787–788 (1933).
22. Ginzburg, V. L. & Andryushin, E. A. *Superconductivity* (World Scientific, 2004).
23. Boltnev, R. E., Vasiliev, M. M., Kononov, E. A. & Petrov, O. F. Formation of solid helical filaments at temperatures of superfluid helium as self-organization phenomena in ultracold dusty plasma. *Sci. Rep.* **9**, 3261 (2019).
24. Lisin, E. A. *et al.* Experimental study of the nonreciprocal effective interactions between microparticles in an anisotropic plasma. *Sci. Rep.* **10**, 13653 (2020).
25. Lisina, I. I., Lisin, E. A., Vaulina, O. S. & Petrov, O. F. Self-confined particle pairs in complex plasmas. *Phys. Rev. E* **95**, 013202 (2017).
26. De Gennes. *The Physics of Liquid Crystals.* International Series of Monographs on Physics. (P. G. Oxford University Press, U.S.A.; 2nd edition, 1995).
27. Takahashi, Y. *et al.* Magnetic trapping of superconducting submicron particles produced by laser ablation in superfluid helium. *Appl. Phys. Exp.* **10**, 022701 (2017).
28. Moroshkin, P., Leiderer, P., Möller, T. B. & Kono, K. Trapping of metallic nanoparticles under the free surface of superfluid helium in a static electric field. *Phys. Fluids* **31**, 077104 (2019).
29. Moroshkin, P., Leiderer, P., Kono, K., Inui, S. & Tsubota, M. Dynamics of the vortex-particle complexes bound to the free surface of superfluid helium. *Phys. Rev. Lett.* **122**, 174502 (2019).
30. Tierno, P. Recent advances in anisotropic magnetic colloids: Realization, assembly and applications. *Phys. Chem. Chem. Phys.* **16**(43), 23515–23528 (2014).
31. Golovashkin, A. I. High-temperature superconducting ceramics (review of experimental results). *Sov. Phys. Usp.* **30**, 659–670 (1987).
32. Kroy, K. & Cichos, F. Hot brownian motion. In *Diffusive Spreading in Nature, Technology and Society* (eds Bunde, A. *et al.*) (Springer, 2018). https://doi.org/10.1007/978-3-319-67798-9_8.
33. Perrin, J. *Atoms* (Constable, 1914).
34. Einstein, A. Über die von der molecularkinetischen Theorie der Wärme geforderte Bewegung von in ruhenden Flüssigkeiten suspendierten Teilchen. *Annalen der Physik: magazin.* **322**(8), 549–560 (1905).
35. Golestanian, R. Anomalous diffusion of symmetric and asymmetric active colloids. *Phys. Rev. Lett.* **102**, 188305 (2009).
36. Jiang, H.-R., Yoshinaga, N. & Sano, M. Active motion of a Janus particle by self-thermophoresis in a defocused laser beam. *Phys. Rev. Lett.* **105**, 268302 (2010).
37. Xiao-Lun, W. & Libchaber, A. Particle diffusion in a quasi-two-dimensional bacterial bath. *Phys. Rev. Lett.* **84**, 3017 (2000).
38. Chopra, K. L. & Brown, J. B. Suspension of particles in liquid helium. *Letters to the Editor. Coll. English* **18**, 373 (1957).
39. Balazs, N. L. Brownian motion of a mirror in superfluid helium. *Phys. Rev.* **109**, 232–234 (1958).
40. Baym, G., Barrera, R. G. & Pethick, C. J. Mobility of the electron bubble in superfluid helium. *Phys. Rev. Lett.* **22**, 20–23 (1969).
41. Zmeev, D. E. *et al.* Observation of crossover from ballistic to diffusion regime for excimer molecules in superfluid 4He. *J. Low Temp. Phys.* **171**, 207–213 (2013).
42. Li, X., Cheng, R., Li, T. & Niu, Q. Brownian motion in superfluid ^{4}He. arXiv:1107.0485 (cond-mat. stat-mech). Preprint at https://arxiv.org/abs/1107.0485 (2011).
43. Donnelly, R. J. & Barenghi, C. F. The observed properties of liquid helium at the saturated vapor pressure. *J. Phys. Chem. Ref. Data* **27**, 1217–1274 (1998).
44. Huang, R. *et al.* Direct observation of the full transition from ballistic to diffusive Brownian motion in a liquid. *Nat. Phys.* **7**, 576–580 (2011).
45. Li, T., Kheifets, S., Medellin, D. & Raizen, M. G. Measurement of the instantaneous velocity of a Brownian particle. *Science* **328**, 1673–1675 (2010).
46. Pusey, P. N. Brownian motion goes ballistic. *Science* **332**, 802–803 (2011).
47. Dombrowski, C., Cisneros, L., Chatkaew, S., Goldstein, R. E. & Kessler, J. O. Self-concentration and large-scale coherence in bacterial dynamics. *Phys. Rev. Lett.* **93**, 098103 (2004).
48. Balykin, V. I., Letokhov, V. S. & Minogin, V. G. Cooling atoms by means of laser radiation pressure. *Sov. Phys. Uspekhi* **28**, 803–826 (1985).
49. Blumenfeld, L. A. *Problems of Biological Physics* (Springer, 1981).
50. Landau, L. Theory of the superfluidity of helium II. *Phys. Rev.* **60**, 356–358 (1941).
51. Vinen, W.F. The physics of superfluid helium. *CAS - Cern Accel. Sch. Supercond. Cryog. Accel. Detect.* 363–373 (2002).
52. Vinen, W.F. An Introduction to Quantum Turbulence. **145**, 7–24 (2006).
53. Feynman, R. P. Chapter II application of quantum mechanics to liquid helium. *Progr. Low Temp. Phys.* **1**, 17–53 (1955).
54. Vinen, W. F. Mutual friction in a heat current in liquid helium II. I. Experiments on steady heat currents. *Proc. R. Soc. Lond. Ser. A* **240**(1220), 114–127 (1957).
55. Vinen, W. F. Mutual friction in a heat current in liquid helium II. II. Experiments on transient effects. *Proc. R. Soc. Lond. Ser. A* **240**(1220), 128–143 (1957).
56. Vinen, W. F. Mutual friction in a heat current in liquid helium II. III. Theory of the mutual friction. *Proc. R. Soc. Lond. Ser. A* **242**(1231), 493–515 (1957).
57. Vinen, W. F. Mutual friction in a heat current in liquid helium II. IV. Critical heat currents in wide channels. *Proc. R. Soc. Lond. Ser. A* **243**(1234), 400–413 (1958).
58. Van Sciver, S. W. *Helium Cryogenics* (Springer, 2012).

59. Mastracci, B. & Guo, W. Exploration of thermal counterflow in He II using particle tracking velocimetry. *Phys. Rev. Fluids* **3**, 1–17 (2018).
60. Guo, W., Cahn, S. B., Nikkel, J. A., Vinen, W. F. & McKinsey, D. N. Visualization study of counterflow in superfluid He4 using metastable helium molecules. *Phys. Rev. Lett.* **105**, 1–4 (2010).
61. Babuin, S., Stammeier, M., Varga, E., Rotter, M. & Skrbek, L. Quantum turbulence of bellows-driven 4He superflow: Steady state. *Phys. Rev. B Condens. Matter Mater. Phys.* **86**, 1–11 (2012).
62. Sergeev, Y. A., Barenghi, C. F. & Kivotides, D. Motion of micron-size particles in turbulent helium II. *Phys. Rev. B Condens. Matter Mater. Phys.* **74**, 2–6 (2006).
63. Tough, J. T. Chapter 3: Superfluid turbulence. In *Progress in Low Temperature Physics* (ed. Brewer, D. F.) 133–219 (North-Holland, 1982).
64. Schwarz, K. W. Three-dimensional vortex dynamics in superfuid He: Homogeneous superfluid turbulence. *Phys. Rev. B* **38**, 2398–2417 (1988).
65. Zhang, T. & Van Sciver, S. W. The motion of micron-sized particles in He II counterflow as observed by the PIV technique. *J. Low Temp. Phys.* **138**, 865–870 (2005).
66. Baggaley, A. W. & Laizet, S. Vortex line density in counterflowing He II with laminar and turbulent normal fluid velocity profiles. *Phys. Fluids* **25**, 115101 (2013).
67. Penney, R. & Hunt, T. K. Particle motion and heat-exchange 'viscosity' in superfluid helium. *Phys. Rev.* **169**, 228 (1968).
68. Kadomtsev, B. B. Dynamics and information. *Phys.-Usp.* **37**, 425–499 (1994).
69. Watari, H., Monjushiro, H., Tsukahara, S., Suwa, M. & Iiguni, Y. Migration analysis of micro-particles in liquids using microscopically designed external fields. *Anal. Sci.* **20**(3), 423–434 (2004).
70. Piazza, R. & Parola, A. Thermophoresis in colloidal suspensions. *J. Phys. Condens. Matter* **20**, 153102 (2008).
71. Varga, E. & Skrbek, L. Thermal counterflow of superfluid 4He: Temperature gradient in the bulk and in the vicinity of the heater. *Phys. Rev. B* **100**, 054518 (2019).
72. Mantese, J., Bischoff, G. & Moss, F. Vortex-line density fluctuations in turbulent superfluid helium. *Phys. Rev. Lett.* **39**, 565–568 (1977).
73. Bohren C.F., & Huffman D.R. Absorption and Scattering of Light by Small Particles. Wiley Science Paperback Series, Chichester, UK (1998).
74. Zött, A. & Stark, H. Emergent behavior in active colloids. *J. Phys. Condens. Matter* **28**, 253001 (2016).
75. Lisin, E. A., Vaulina, O. S., Lisina, I. I. & Petrov, O. F. Active Brownian particle in homogeneous media of different viscosities: Numerical simulations. *Phys. Chem. Chem. Phys.* **23**(30), 16248–16257 (2021).
76. Reimann, P., Grifoni, M. & Hänggi, P. Quantum ratchets. *Phys. Rev. Lett.* **79**, 10–13 (1997).
77. Parrondo, J. M. R. & De Cisneros, B. J. Energetics of Brownian motors: A review. *Appl. Phys. A* **75**, 179–191 (2002).
78. Volkenstein, M. V. *Entropy and Information* (Birkhäuser, 2009).
79. Varga, E. Peculiarities of spherically symmetric counterflow. *J. Low Temp. Phys.* **196**, 28–34 (2019).

Acknowledgements

We thank E.A. Lisin for helpful discussions. The work has been carried out under the support of the Russian Science Foundation (Project # 20-12-00372).

Author contributions

O.F.P. developed the concept, analyzed the results, and wrote the main manuscript with assistance provided by the coauthors. R.E.B. and M.M.V. carried out the experiments data collection and prepared all figures and videos. M.M.V. performed statistical analysis of grain motion. All authors discussed and reviewed the manuscript.

Competing interests

The authors declare no competing interests.

Additional information

Supplementary Information The online version contains supplementary material available at https://doi.org/10.1038/s41598-022-09523-z.

Correspondence and requests for materials should be addressed to O.F.P.

Reprints and permissions information is available at www.nature.com/reprints.

Publisher's note Springer Nature remains neutral with regard to jurisdictional claims in published maps and institutional affiliations.